Influence of atmospheric circulation and local parameters on activity concentration of gross alpha and gross beta in Granada, Spain

Influence of atmospheric circulation and local parameters on activity concentration of gross Alpha and gross Beta in Granada, Spain

I. Berriban[a], E.Chham[a,b], Abdelhamid Nouayti[a], M. Azahra[a], J.A.G. Orza[b], H. Ziani[a], T. El Ghalbzouri[a], T. El Bardouni[a], M. Hadouachi[a], A. Milena-Pérez[c], F. Piñero-García[d], L. Tositti[e], E. Brattich[f], I. Ben Maimoun[g], and M.A. Ferro-García[d]

[a]*Radiations and Nuclear Systems Group, FS, Abdelmalek Essaadi University, Tetouan, Morocco*

[b]*SCOLAb, Fisica Aplicada, Miguel Hernandez University, Elche, 03202, Spain*
[c]*Centro de Investigaciones Energéticas, Medioambientales y Tecnológicas (CIEMAT), Madrid, 28040, Spain*

[d]*Radiochemistry and Environmental Radiology Laboratory, Inorganic Chemical Department, Faculty of Sciences, University of Granada, Granada, 18077, Spain*

[e]*Department of Chemistry 'Giacomo Ciamician', Alma Mater Studiorum, University of Bologna, Via Francesco Selmi 2, Bologna, 40126, Italy*
[f]*Department of Physics and Astronomy, University of Bologna, 40126, Bologna, BO, Italy*
[g]*Water, Environmental Studies and Analysis laboratory, Inorganic Chemical, FS, Abdelmalek Essaadi University, Tetouan, Morocco*

Abstract

This work analyses the influence of local meteorology and air mass origin on radioactivity levels measured in Granada (Southern Spain). To the scope, gross α and gross β activities at ground-level air were weekly recorded from 2006 to 2021, by collecting aerosol filters and successively analysing them by low-level proportional counting. Time series decomposition shows a strong correlation between the seasonal components of gross α and gross β and the local meteorological parameters, in particular temperature and wind speed. Back trajectories reaching the study area during the sampling, calculated at three height levels (750m, 1500m, and 3000m a.s.l.), were analysed by three methods with the aim to determine the main characteristics of air masses reaching Granada, and their impact on airborne radioactivity levels. The results of the residence time and clustering analyses showed that an increase in the radioactivity levels in the southeast of Spain is connected with air masses coming from the Mediterranean at 750 m and from the South (Sahara Desert) at 3000 m. In line with the outcomes obtained by the cluster analysis, the Concentration Weighted Trajectory (WCWT) results highlight that the air masses transported from Mediterranean and African regions are a potential source of gross α and gross β. Moreover, the findings of the WCWT bring a new aspect by revealing that the southern France region can also have a significant contribution to gross alpha and beta activities.

Keywords: Gross Alpha, Gross Beta, Air masses, Back-trajectories, Radioactivity.

1. Introduction

Natural radioactivity in air is explained by the presence of cosmic radiation which generates cosmogenic radionuclides (e.g. ^{14}C, ^{7}Be, and ^{3}H), and the release of some naturally occurring radionuclides from the Earth's crust to the atmosphere, mainly represented by ^{222}Rn from the ^{238}U family, and its progeny (Chambers et al., 2017, 2018; Brattich et al., 2016, 2017; Papastefanou, 2008; Piñero-García et al., 2015). Although atmospheric radioactivity is generally controlled by natural sources and dilution (atmospheric mixing depth and dispersion), atmospheric radioactivity levels can typically fluctuate as a result of atmospheric circulation, but may occasionally increase either due to natural processes or to anthropogenic sources, such as from nuclear accidents, nuclear weapon tests, nuclear energy production, etc . Most of airborne radionuclides are associated with aerosol particles whose size distribution ranges between the nanometer and the tens of micrometer size (Papastefanou, 2008). Similarly, to stable aerosol species, particle size distribution controls the size distribution of airborne particle-reactive radionuclides, affecting their atmospheric residence time (which for radionuclides depends also on their physical lifetime), and consequent environmental fate, including respirability and therefore inhaled doses. Therefore, monitoring radioactivity levels in the ambient air is mandatory in order to ensure the protection of human health. In addition, the study of atmospheric radioactivity has been historically widely applied as a way to analyze short, medium, and large-scale atmospheric transport processes (Chambers et al., 2017, 2018; Brattich et al., 2021; Hirose, 2012; Lee et al., 2007; Sykora and Klaus, 2009; Turekian and Graustein, 2003).

^{222}Rn is a gaseous radionuclide that forms naturally from the decay chain of ^{238}U and has a half-life of 3.8 days. ^{222}Rn has several daughters, such as ^{218}Po (3.1m, α);^{214}Pb (27m, β); ^{214}Bi (20m, β);^{214}Po (160μS, α); ^{210}Pb (22.3 years, β−); ^{210}Bi (5 days, β−); and ^{210}Po (138 days, α); These emitters represent a potential hazard of internal contamination, especially if ^{222}Rn and descendants are inhaled. Although the shorter-lived progeny may have higher immediate activity levels, their shorter half-lives mean that they decay relatively quickly, reducing their long-term impact. Conversely, radon progeny with longer half-lives, such as ^{210}Pb, can persist in the atmosphere for longer periods of time and potentially be transported over longer distances, resulting in more widespread exposures (World Health Organization, 2009). Several studies have been conducted on radon in Spain, addressing various aspects of the topic. For instance, (Fernández et al., 2021; García-Talavera and Acevedo, 2019) focused on identifying the areas in Spain that are exposed to radon, creating a radon potential map. (Vargas et al., 2015) studied the vertical radon structure in the southwest of the Iberian Peninsula.

Furthermore, radon as a noble gas directly emits its alpha emissions in the gas phase while its progeny, highly particle-reactive, interacts by association with the carrier aerosol in the particulate phase. As such, they are considered the main contributors to the gross α and gross β activities measured in air (Sáez-Muñoz et al., 2018). These parameters are usually used as indicators useful to promptly detect unusually high

levels of radioactivity records in the atmosphere, at the basis of efficient alerting initiatives by environmental radiological surveillance. As a result, extensive radioactivity databases are available worldwide enabling to successfully perform different modelling studies. The long-term monitoring of atmospheric gross α and gross β activities concentration allows the analysis of temporal trends, periodicities, and influencing variables. In particular, gross α and gross β are highly affected by meteorological parameters, such as precipitation and relative humidity which control the wet removal of the particulate phase to which most of the airborne radionuclides are associated, as well as air temperature, atmospheric pressure, wind speed, wind direction, i.e. the parameters driving atmospheric circulation. A number of studies have been carried out regarding weekly measurements of gross α and gross β variations in several sites of Spain; such as North West by (García-Talavera et al., 2001), and in South East by (Sáez-Muñoz et al., 2018). They provided detailed information about the impact of meteorological conditions at their sampling sites based on the gross α and gross β concentrations in surface air. In Malaga, South of Spain, (Cabello et al., 2018) studied the influence of air mass circulation on the variations of gross α and gross β concentrations, and conclude that the African air masses at 3000 m a.s.l. and Mediterranean flows at 500 m are related to high gross α and gross β activities. Similar conclusions were obtained also by (Piñero-Garcíaet al., 2015) who indicate that radioactivity levels in aerosols at their study site are increased by long-range air masses transported from Africa suggesting an influence of local geological background.

In this work, the measurements of gross α and gross β in Granada over 16 years (2006–2021) are used as a large database to obtain more robust conclusions about their temporal behavior. The main aim is thus to identify the synergism between atmospheric transport features factors and natural radioactivity background on the variability of gross α and gross β activities. For this purpose, the concentrations of gross α and gross β radiation data collected on a weekly basis at Granada (Spain) over the study period were studied by means of several methods including time series and back-trajectory analysis.

All in all, the specific goals of this study are to:

- Interpret the variability of gross α and gross β time series.
- Examine the influence of atmospheric parameters on different components of time series, using the Time Series Decomposition (TSD) technique.
- Extract the periodicities in time series by using the Continuous Wavelet Transform (CWT) analysis.
- Investigate the principal sources areas for α and gross β activities in air masses using clustering analysis of air masses back trajectories and Weighted Concentration Weighted Trajectory (WCWT) Model.

2. Data and methodology

2.1. Description of data site and radiometric analysis

The current research was carried out in Granada for 16 consecutive years 2006 to 2021. This city is located in the South of Spain, bounded in the West by the provinces of Malaga and Cordoba, and in the North by Jaen province. It has a continental Mediterranean climate, relatively hot and dry in summer due to the protection of the winds from the tip of the Sierra Nevada, and cold winters resulting from the city's location in the foothills of Sierra Nevada at an altitude of 680 m asl. (Piñero-García and Ferro García, 2014). Granada is frequently affected by huge Saharan dust events because of the limited distance from the African continent, of the order of 200 km (Guerrero-Rascado et al., 2009). These events result in sudden increases in particulate matter concentrations, together with significant physico-chemical changes in the surrounding atmosphere, due to the hygroscopic characteristics and high mineral content of the dust particles (Titos et al., 2014; Morozzi et al., 2021).

The sampling station is located on the rooftop of the Faculty of Sciences of the University of Granada (37.177N, 3.598 W, 680 m a.s.l.), where the Radiochemistry and Environmental Radiology Laboratory is situated. Airborne PM10 samples were collected weekly on cellulose filters, 47mm diameter and 0.8 mm effective pore size, by using an air sampler RADECO, model AVS-28A. The air sampler worked with a flow rate of 85 L/min, collecting an approximate volume of 800m^3 per week. After sampling, the filters were stored in desiccators inside Petri dishes until the measurement, in order to prevent contamination of the samples. The total covered period ranges from January 2006 to December 2021, thus giving a total sampling coverage of 16 years with 864 filters. The gross α and gross β indexes were measured in the collected filters by using the proportional counter Berthold LB -770-2/5. The detection system was equipped with 10-channels, which allows us to measure 10 samples simultaneously. Each filter is placed on a stainless steel planchet during a measurement time of 1000 minutes. The radionuclides ^{241}Am and ^{90}Sr, as standard sources of α and β emitters, respectively, were employed to calibrate the instrument. The system performance was verified by measuring standard samples prepared by the CIEMAT Ionizing Radiation Metrology Unit. Background contributions and limits of detection of the instrument have also been evaluated in order to ensure the results at every moment.

2.2 Studied variables

In this work, the following meteorological parameters, provided by the Spanish National Institute of Meteorology, AEMET, were analysed: air temperature (T)(ºC), relative humidity (RH%), wind speed (WS)(km/h), precipitation (Pp)(mm), and pressure (Pr)(bar). In order to homogenize the time series with the time resolution of radioactivity levels, the original daily measurements of temperature, humidity and

wind speed were transformed to average weekly values. weekly precipitation totals calculated from daily precipitation data were used due to the typical rainfall regime in Granada, characterized by torrential rainfall on a few days and dry weather on others (Piñero-García et al., 2015).

2.3 Time Series Decomposition (TSD)

Time series data can display different patterns; it is convenient to split a time series into distinct components, each one representing a different type of underlying pattern. There are several procedures that can be applied to analyse a time series (see e.g., Scott and Richard 2011). In this work, additive Time Series Decomposition (TSD) was used to detect the intrinsic dynamics of gross α and gross β time series, as well as to investigate the link of each component with different meteorological factors. Therefore, three independent components were estimated.

- Trend component (T_t), which presents the long-term behavior of the time series. It can be increasing, decreasing, or stationary in the mean.
- Seasonal component (S_t) reflects sub-annual fluctuations in a time series. It displays regular patterns during a given period of time (in this study such a period is one year).
- Irregular (R_t) or unpredictable component, describes the random factors affecting the behavior of the time-dependent variable after detrending and removal of seasonal components.

Based on the TSD, the data studied can be defined as:

$$Y_t = T_t + S_t + R_t \quad (1)$$

where (Y_t) are the observations.

TSD method identifies the trend component based on a centered moving average filter of order 12. This component is subsequently removed from the original time series. The seasonal pattern is determined using the average of the detrended gross α and gross β activities concentration in each month, taking into account the 16 years of measurements. Finally, the irregular component is calculated by subtracting the trend and seasonal estimates.

2.4 Continuous Wavelet Transform (CWT) analysis

The Continuous Wavelet Transform (CWT) method is a useful technique to analyze time series that include non-stationary power at many different frequencies (scales) (Daubechies, 1990). Here, wavelet power spectra were computed by the Morlet wavelet transform, defined as a harmonic wave with a frequency, containing a plane wave modulated by a Gaussian:

$$\Psi_0(n) = \pi^{\frac{-1}{4}} e^{-i\omega_0\eta} e^{\frac{-\eta^2}{2}} \quad (2)$$

In the above relation, ω_0 is a dimensionless frequency, η is the non-dimensional time parameter, and $\Psi_0(n)$ is the basic wavelet function. Assuming a time series X with values x_n, uniform time spacing δ_t, and time index n = 0, …, N-1, the continuous wavelet transform of this time series is defined as the convolution of the scaled wavelet function with the original time series:

$$W_n(s) = \sum_{n'=0}^{N-1} x_{n'} \Psi * \left[\frac{(n'-n)\delta t}{s}\right] \quad (3)$$

Where, Ψ is defined as a normalized function of a wavelet function Ψ_0. The asterisk indicates the complex conjugate, s stands for the scale, n′ refers to the time translation, and N is the length of the time series. Based on Equation (3), calculation of the continuous wavelet transform is possible, but it is highly time consuming. Nevertheless, Equation (4) becomes faster using the convolution theorem (Fourier space) as below (see (Keim et al., 2004) for further details):

$$W_n(s) = \sum_{n'=0}^{N-1} \hat{x}_k \hat{\Psi} * [s\omega_k] e^{i\omega_k n \delta t} \quad (4)$$

2.5 Trajectory database, residence time, and clustering analysis

The analysis of back-trajectories provides information on the dispersion/recirculation of substances in the atmosphere, as well as studies the origin and history of the air masses reaching a particular sampling site.

In this work, the meteorological database used as input for the trajectory calculation is ERA-Interim, interpolated to 0.5 deg horizontal resolution, from the European Centre for Medium-Range Weather Forecasts (ECMWF). Specifically, 96h kinematic 3D back-trajectories, were calculated 4 times per day, every 6 hours at 00:00, 06:00, 12:00 and 18:00 (UTC). In addition, three altitudes above sea level (a.s.l) have been considered over the study site: 750m (within the planetary boundary layer), 1500m (about the upper limit of the boundary layer), and 3000m (free troposphere). The back-trajectories calculation was performed using the Hybrid Single-Particle Lagrangian Integrated Trajectory (HYSPLIT) model (Draxler et al., 2009).

The time spent by the air parcels reaching the study site over different regions was calculated by counting the number of end-points (one per hour) that lie within each region. The primary regions of interest are the continental and oceanic areas, each as a whole and then disaggregated as the Atlantic, the Mediterranean, continental Europe, and continental Africa. Subsequently, the association between residence times and concentration activities was analysed.

Cluster analysis is a common statistical technique used to partition datasets (a set of trajectories) into homogeneous subgroups or clusters. The similarity metrics implemented in HYSPLIT is based on the Euclidean distance between trajectories, using the following equations:

$$d_{mi} = \sqrt{\sum_k^n (lat_{mk} - lat_{ik})^2 + (lon_{mk} - lon_{ik})^2} \quad (5)$$

$$CSV_m = \sum_{i=1}^{c} {d_{mi}}^2 \quad (6)$$

$$TSV = \sum_{m=1}^{N} CSV_m \quad (7)$$

Where d_{mi} is the Euclidean distance between the i^{th} trajectory and the mean trajectory (or cluster-mean, m), n is the number of endpoints in a trajectory, *lon* and *lat* are the longitude and latitude values, respectively, at the endpoints (m, k) and (i, k). CSV_m is the Cluster Spatial Variance for the m^{th} cluster; c is the number of trajectories in the cluster m. Finally, TSV accounts for the Total Spatial Variance and N is the number of clusters.

This method works following an iterative procedure. First, the number of generated clusters is equal to that of the trajectories. After each iteration, two clusters are merged together, until only two clusters remain. As the merging criteria, all the possible combinations are tested according to the TSV value, in such a way that the combination with the minimum TSV is retained for the next iteration. The final clustering solution is the one with a number of clusters for which the TSV does not start to increase as the clusters are merged into a few.

2.6 Weight Concentration Weighted Trajectory (WCWT) Mode

After calculating the trajectories reaching the sampling site, WCWT analysis has been carried out to identify potential source areas of α and β emitters comprised in the gross α and gross β activities. This was accomplished by combining back trajectories with the measured activity concentrations. The full geographic region covered by the air-mass trajectories is gridded into small cells (i, j) with a resolution scale of 0.5º × 0.5º (Cheng et al., 2013) and the residence time of each trajectory over each grid cell is obtained. Then C_{ij}, the average weighted concentration in the i_{th} cell, as follows:

$$C_{ij} = \frac{1}{\sum_{l=1}^{M} \tau_{ijl}} \sum_{l=1}^{M} C_l \, \tau_{ijl} \quad (8)$$

where l is the index of the trajectory, M is the total number of trajectories, C_l is the concentration pointed on the arrival of trajectory l, and τ_{ijl} refers to the time spent in the ij^{th} cell by trajectory l. To reduce the effect of small values of C_{ij}, an arbitrary weight function W_{ij} was multiplied to minimize the uncertainty in the values for these cells.

$$W_{ij} = \begin{cases} 0.7 if 30 \le n_{ij} \le 50 \\ 0.7 if 15 \le n_{ij} \le 30 \\ 0.05 if 0 \le n_{ij} \le 15 \end{cases} \quad (9)$$

Therefore, the Weight Concentration Weighted Trajectory is defined as:

$$WCWT = W_{ij} \times C_{ij} \quad (10)$$

3. Results and Discussion

3.1 Gross α and gross β activities: Time Series

Figures 1(a,b) shows the weekly evolution of gross α and gross β activities in the atmosphere. The evolution of both parameters indicates a cyclical pattern corresponding to the annual variation. This variability over the seasons is mainly explained by atmospheric factors (Sáez-Muñoz et al., 2018). The highest gross α and gross β activity concentrations were recorded in summer (between June and September) while the lowest values were measured in winter. This observation can be explained by the increased dryness and the intense convection promoting both radon exhalation and soil resuspension through turbulence and significant vertical uplift of aerosol particles (Berriban, et al., 2022; Brattich, et al., 2020; Hernández-Ceballos et al., 2022; Lee, 2007; Tositti, et al., 2014). Thus, this phenomenon increases the airborne levels of gross α and gross β emitters, and therefore the values of gross α and gross β as a result of the enhanced crustal contribution of both gaseous and particulate natural radionuclides.

Figure 1 (c) presents the superimposed plot of the monthly average alpha and beta activities. In general, the evolution of both indexes presents a similar pattern over the years. However, during some years, the curves are quite different. The variations in patterns between gross alpha and gross beta activities observed during specific years can be attributed to a combination of several factors. These include the presence of different radioactive isotopes contributing to each activity index (Hernándezet al., 2005), temporal variations in emission sources, environmental factors such as weather patterns and precipitation, locality of the sampling point and the history of the air mass. (Terrayet al., 2020). Indeed, the occurrence of these anomalies still needs more studies to be evaluated. The activity concentrations of both gross α and gross β ranged from 0.015 ± 0.002 mBq/m^3 to 0.422 ± 0.133 mBq/m^3, and from 0.034 ± 0.003 mBq/m^3 to 1.100 ± 0.017 mBq/m^3, respectively, and the mean values determined over these years are 0.163 ± 0.007 mBq/m^3 and 0.499 ± 0.008 mBq/m^3. Similar pattern has been reported in other locations of the Iberian Peninsula such as Salamanca or Málaga (Dueñaset al., 2011a). To provide a complete statistical comparison, box, and whiskers plots are also displayed in Figure 1. The median value is 0.142 ± 0.007 mBq/m^3 for α and 0.476 ± 0.007 mBq/m^3 for β, not significantly different from the mean values. The symmetry of the box with respect to the middle line suggests that gross β radiation follows symmetry in the frequency distributions, therefore, it has a normal distribution. On the contrary, gross α activities follow a log-normal distribution.

In order to support this assessment, the Kolmogorov-Smirnov test has been applied. The test confirms that normal distribution is the best fit for the evolution of gross β, with a significant p-value higher than 0.05 (0.073). Conversely, the log-normal distribution is suitable for gross α with a significant p-value of 0.4518.

Log-normality has been widely observed for both indoor and outdoor radon which may be substantially represented in gross alpha radiation, in agreement with (Bossew, 2010) on the basis of the physical phenomenology of radon emission. As concerns the normal distribution of gross beta, this issue would require an in-depth investigation, which is beyond the scope of this paper.

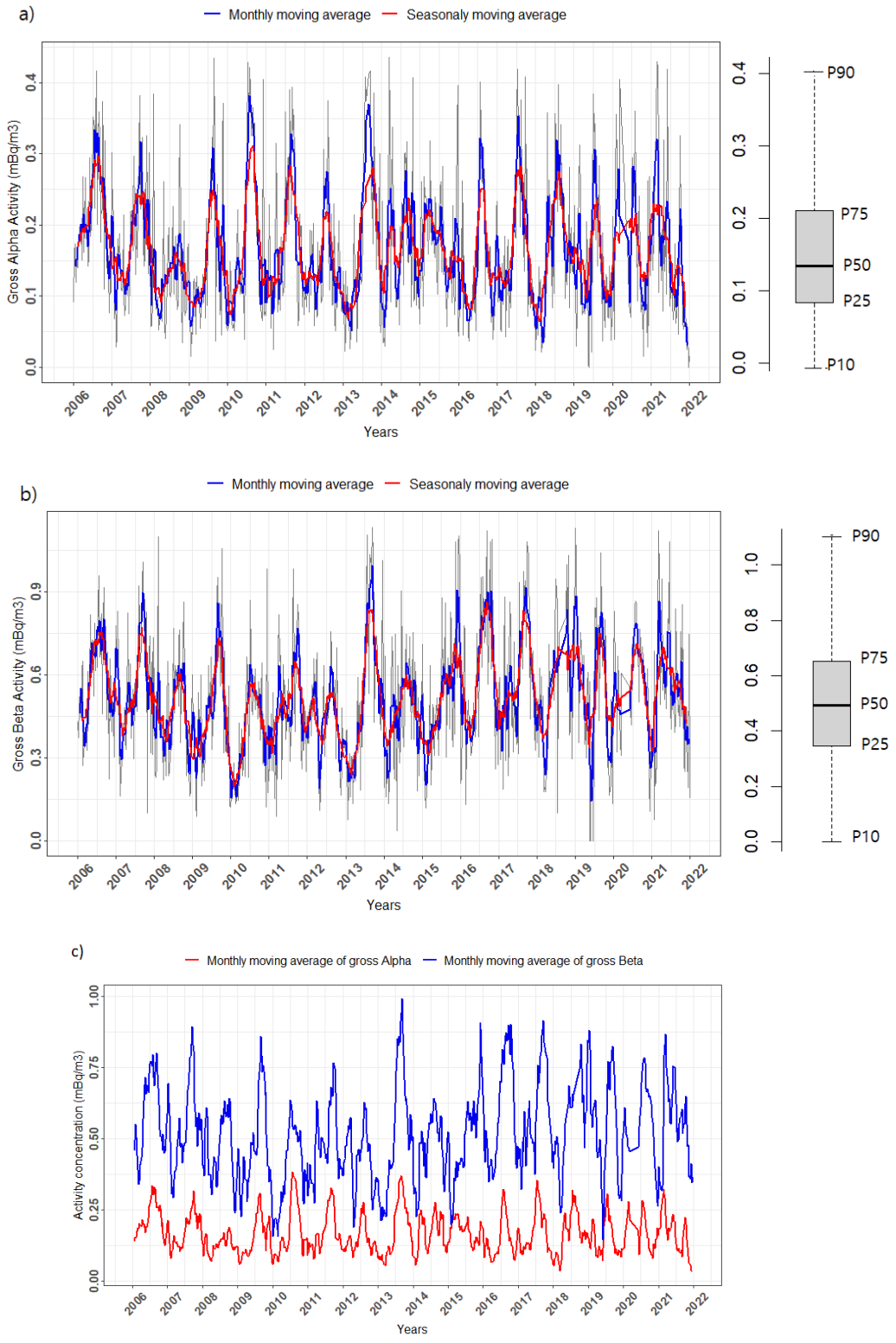

Figure 1: Temporal variation of (a) gross α and (b) gross β activity concentrations, including seasonally and monthly averages, for the period 2006-2021. Box and whiskers are added at the right, (c) supposed plot of monthly moving average of both indexes.

3.2 Influence of local meteorological parameters in gross α and gross β activities concentration

3.1.1. Decomposition Time Series of gross α and gross β activity concentrations

According to the TSD method previously described, gross α and gross β time series were decomposed into three independent components namely trend, seasonal, and random components. As a complement, the multiple regression analysis was used to determine the relative importance of each component in gross α and β variability, attending to standardized coefficients of each component (Baset al., 2016). The relative importance of the Trend component is 9% and 16% for gross β and gross α, respectively, for the Seasonal component it accounts for 42% and 41%. The Random Component represents 49 % and 43 % of gross β and gross α, respectively.

In order to get a clear idea of the underlying patterns and fluctuations in gross α and gross β activities, various graphs are presented in Figure 2. Figure2 (a, b) illustrate the trend, while Figure2 (c, d) represent the data with the trend removed. Finally, Figure2 (e, f) show the single composite year for gross α and gross β, respectively.

As shown in Figure 2(a, b), An inter-annual variability is clearly displayed. Generally, a clear positive trend can be observed for gross β compared to gross α, which instead shows a slightly decreasing behavior. Figures 2 (c, d) shows the seasonal pattern of gross α and gross β over the sampling period. This seasonality becomes very clear in Figures 2 (e, f), where weekly mean values of gross α and gross β over the sampling periods are plotted. These figures highlight the intra-annual variability of gross α and gross β. It can be seen that the highest activity concentrations in gross α and gross β were recorded during the summer (between weeks 25^{th} and 45^{th}), while the lowest values were measured during the remaining seasons of the year, especially in winter.

However, the relative importance of the time series components of gross α and gross β activity concentrations data present some inconsistencies over the period study. This variability is represented by the irregular component (which is obtained by the subtraction of the composite seasonality from each year observations), which reflects the fluctuations observed due to some events such as sudden changes in climatic factors (wind speed, temperature, air pressure and precipitation, etc.). Where, the large contribution of the "random" component is probably due mainly to the synoptic time scale at this site, which is shorter than the integration period of the measurements. This means that large-scale weather events occur frequently and rapidly at this site, resulting in significant random fluctuations in the measurements.

The trend component is characterized by a feeble relative importance; however, the seasonal and random components have a strong influence on gross α and gross β variability. Therefore, it is essential to analyze in more depth their connection with atmospheric parameters to detect sources of variability that explain

gross α and gross β activities. Due to the nature of each component, the pattern of random component is difficult to interpret, as it is a result of unforeseen events. Thus, more efforts have been put in analysing the variability of the seasonal component.

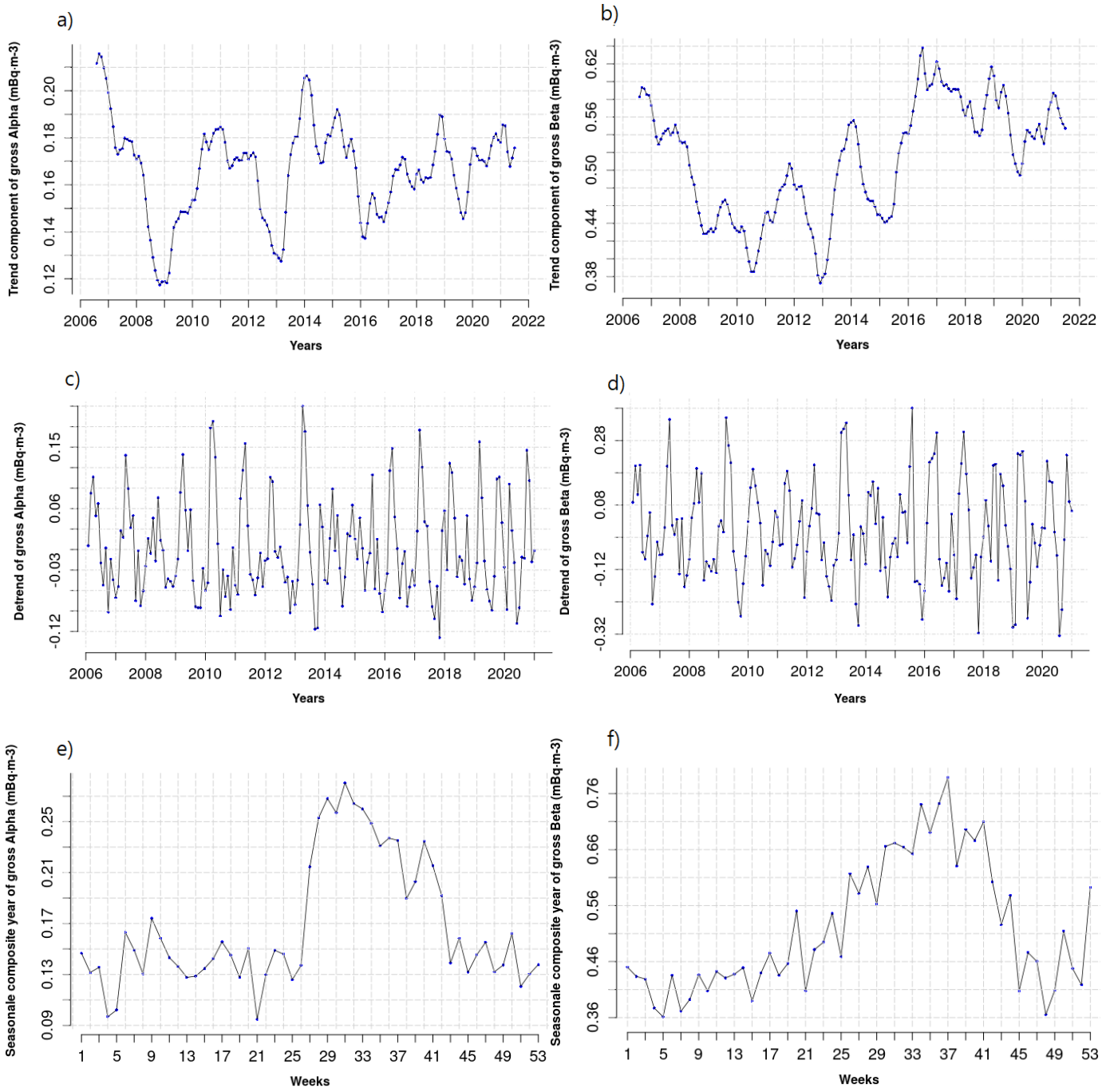

Figure 2: Trend (a, b), Detrend (c, d) and Single composite year (e, f) obtained by decomposition of gross α and gross β time series over the period 2006-2021.

3.1.2. Correlation of gross alpha-beta and the meteorological parameters.

In the current section, we will focus on the impact of the local meteorological parameters (T, RH, WS, Pr, and Pp) on the different components (Trend, Seasonal, and Random components). Spearman's and Pearson

linear correlations of gross α and gross β activities and the time series components with atmospheric parameters are given in Figure 3.

The results show that the trend and irregular components of gross α and gross β present a weak correlation with atmospheric parameters. However, the seasonal component presents a moderate correlation with some of the studied parameters. For this reason, in the following, we will focus on this component. There is a relatively strong (both positive and negative) correlation with Temperature and wind speed, and a weak correlation with the remaining parameters.

In the case of temperature (T), there is a clear positive correlation, r = 0.19 for gross α and r = 0.47 for gross β. If one compares this value with other studies performing a similar correlation study, there is a clear agreement with some of them, e.g., correlation coefficients ranging from 0.18 to 0.36, and from 0.11 to 0.63, for gross α and β, respectively (Dueñas et al., 1999; Hernández et al., 2005; Sáez-Muñoz et al., 2018). The temperature gradient can influence atmospheric stability. Basically, these processes are sub-daily and are captured by hourly data and we have weekly data. Therefore, this mechanism is not dominant on a weekly basis. But also, other synoptic conditions wherein gradients in T and Pressure may affect large-scale transport from areas with larger radon potential. Furthermore, several factors may contribute to the apparent positive correlation between temperature and gross α and gross β. On seasonal timescales, the radon source function is larger in summer, and nocturnal mixing depths are often shallower in summer. These two factors combine to result in higher concentrations of gross α and gross β activities (Reiter and Munzert, 1982). Additionally, the air originating from oceanic regions is highly depleted in radon as compared to continental ones, owing to emanation fluxes less than 1%. Conversely, air from terrestrial regions is typically warmer and drier, with high levels of radon progeny. Therefore, while a positive correlation with temperature has been observed, it is more likely that the reason is related to the surface characteristics of the fetch region.

Concerning the wind speed (WS), it is also influencing gross α and β activities but negatively (r = −0.35 and -0.27, respectively). These coefficients are also found in other cities (Dueñas et al., 1999; Hernández et al., 2005). This relationship is explained by the behavior of wind, which increases the dilution and the dispersion effects leading to the decrease of aerosol-borne radioactivity.

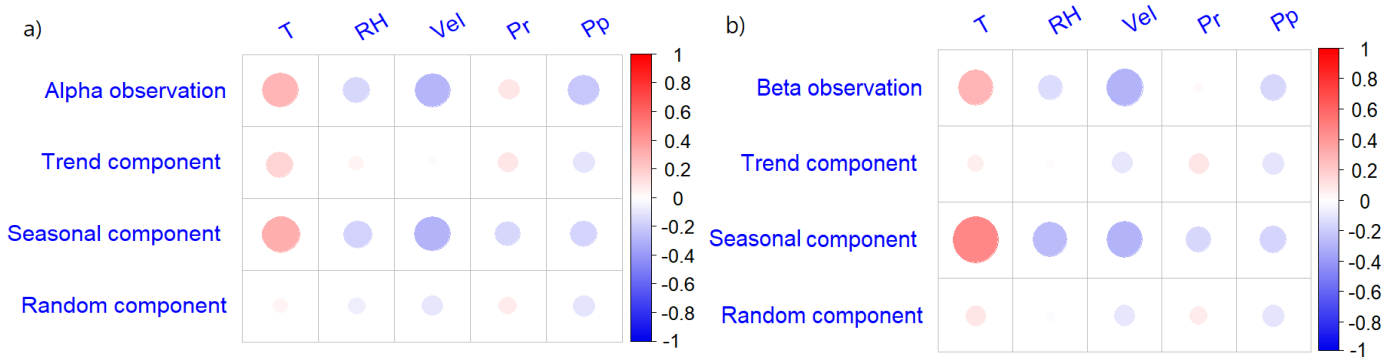

Figure 3: Spearman's and Pearson correlation of (a) gross α and (b) gross β observations, trend, seasonal and random components with the meteorological parameters and teleconnection indices during the study period (2006–2021).

3.1.3. Periodicities in gross α and gross β activities data

In order to understand the monthly variability of gross α and gross β activity concentration between 2006 and 2021, Continuous Wavelet Transform (CWT) analysis was carried out using the 'Morlet' wavelet. The CWT investigates the inter-annual periodicities in the gross α and gross β time series. Figure 4 displays the local wavelet power spectra of the monthly gross α and gross β time series. In the Figure, the x-axis represents the study period and the y-axis represents the time scale of a periodicity, where the unit is 1 month. The existence of a region enclosed by a thick dark contour confirms, at the 5% confidence level, when tested against red noise, the presence of periodicity at time scales that are read in the y-axis, with a period of time covering the number of years that can be read on the x-axis. There are two types of periodicities, strong and intermittent. The strong and stable periodicity of time-series presents continuous bands at a certain period. However, the intermittent periodicity is explained by the presence of 'islands', where power fluctuates above and below the noise level. Results in the so-called cone of influence are potentially affected by artifacts due to the finite length of the time series and are not considered.

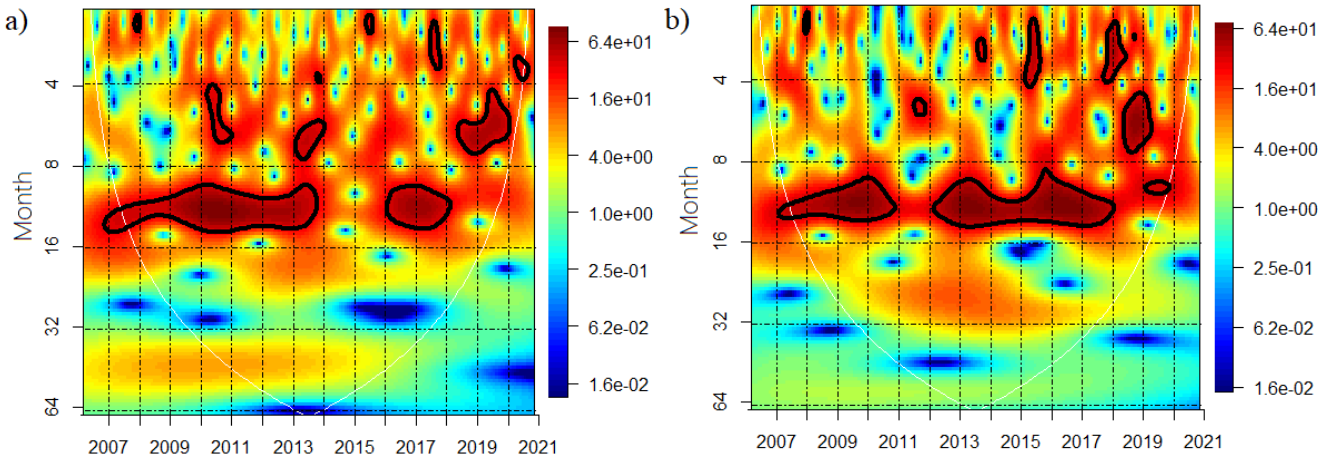

Figure 4: CWT analyses (a) of gross α and (b) gross β time series. The bar on the right denotes the wavelet power (colored shading). Significant periodicities at the 5% confidence level, tested against red noise, are indicated by thick black contours. The cone of influence is under the U-shaped white line.

The different sets of periodicities for each data were represented by the CWT analysis during the 16 years studied. For gross α data, the CWT analysis finds periodicities at the 1-4, 4-7, 6-8, and 10-14 month scale. In gross β data, the periodicity occurs at 1-4, 4.5-7.5, and 10-14 month scales. The strong periodicity observed for 10-14 months suggested that gross α and gross β activity concentrations have a recurrent pattern corresponding to the expected annual variation observed also in airborne radionuclides determined in gamma spectra of atmospheric filter samples (Xianhua et al., 2021; Yasin et al., 2020; Renjie et al., 2013). Periodicities around 6-month can be related to the similarities in temperature and rainfall in spring and autumn, while other inter-seasonal periodicities larger than one month are a combination of several meteorological factors difficult to identify.

As shown in Figure 3, a specific trend (inter-cycles) of gross α was noted between 2009-2013 and 2013-2016. The same behavior was also observed in the gross β trend between 2007 and 2020, where several inter-cycles of two years appeared (2007-2009, 2009: middle of 2010, 2010-2013, 2013-2015, middle of 2018-2020) which could be related to the influence of the Quasi-Bienial Oscillation (QBO) at the lower stratosphere in midlatitudes through instabilities propagating down to the troposphere. Therefore, the periodicity estimated of gross α data is ranged from 36 to 48 months scales and 24 months scales from gross β. However, the CWT results show unexpected periodicities of both data sets. The strong periodicity appears from 10-14 months scales stretching between 2008-2014 and 2016-2018 for gross α time series. As for gross β, this periodicity is extended from 2006 to 2011 and from 2012 to 2018. These unforeseen results may be explained by the poor relative importance of the trend component which includes only 9% and 16.23% for gross α and gross β respectively.

3.3 Impact of air masses on gross α and gross β activities.

The air masses reaching Granada are analysed by means of back-trajectories clustering methods. The purpose is to assess the origin, pathways, and frequency of air mass transport affecting Granada in the investigated period, as well as to identify which air masses are connected with the increase in the radioactivity levels in the atmosphere. The analysis of air masses has been carried out by dividing the data set into six activity concentration ranges of gross α index (being the same for gross β) at three different altitudes: 750m, 1500m, and 3000m a.s.l. (Ac<10P, [10P<Ac<25P], [25P<Ac<50P], [50P<Ac<75P], [75P<Ac<90P], and Ac>90P).

The residence time over marine environments, before passage over the study site close to the surface, is associated with any of the activity concentration ranges, with slightly higher residence time for both the lowest and highest 10th percentiles (Table 1). However, it is clearly observed that while air parcels residing previously over the Atlantic present the lowest concentration activities, the ones residing over the Mediterranean are associated with the highest concentrations. Oceanic air is a poor source of gross α and gross β, but the Mediterranean shows a continental-like behavior due to the accumulation and ageing of a number of compounds of continental origin, as will be discussed later on.

Continental transport to Granada at low levels is complementary to the transport from marine environments shown in Table 1, with a low association between residence times and activity concentrations but slightly lower times are associated with the highest and lowest activity concentrations. Disaggregation between European and African gives no further insight. In turn, the air parcels residing over North Africa and reaching the study site at higher altitudes (3000 m) do show a significant increase in activity concentrations. This height is within the altitude range of advected dust-laden layers of African air masses in the study area. Particle settling and entrainment into the atmospheric boundary layer allows detection at the ground level in the study site.

Table 1: Percentage of back trajectories (columns on the left) and hours (columns on the right) residing over some specific regions by gross α and gross β activity concentration ranges. The table shows only selected results for 750 and 3000 m.

		Trajectories (%)				Hours (%)			
	Activity	**Over the sea**	**Mediterranean**	**Atlantic**	**Over Africa**	**Over the sea**	**Mediterranean**	**Atlantic**	**Over Africa**
α	**P10**	98.3	26.9	91.8	16.7	60.5	8.6	51.9	5.0
	P10/25	96.4	31.9	88.1	24.1	52.9	12.8	40.0	8.8
	P25/50	95.6	46.7	75.4	28.9	51.5	22.9	28.6	12.4
	P50/75	96.4	58.7	64.8	35.4	54.0	29.8	24.2	15.2
	P75/90	97.4	70.4	57.8	38.5	55.0	34.0	21.0	17.8
	P90	97.2	83.3	39.3	48.4	59.6	42.8	16.8	23.8
β	**P10**	98.4	26.9	91.8	14.8	59.8	7.6	52.2	4.8
	P10/25	97.4	31.9	88.1	19.1	53.7	10.6	43.1	6.3
	P25/50	96.5	46.7	75.4	28.9	52.9	21.8	31.1	11.5
	P50/75	95.3	58.7	64.8	34.4	52.3	29.0	23.3	14.7
	P75/90	96.6	70.4	57.8	46.1	55.7	37.4	18.2	23.5
	P90	96.8	83.3	39.3	53.3	58.1	47.0	11.1	23.7
			750 m		**3000 m**		**750 m**		**3000 m**

Figure 5 and Figure 6 present the cluster analyses of the back-trajectories for the six ranges of gross α and gross β activities at the studied altitudes. Taking as a reference the origin and pathway of air masses, different clusters have been identified for each altitude: West (W), Northwest (NW), North (N), Arctic (Ar), South (S), and Mediterranean (Med). These clusters can be classified as fast or slow depending on the distance covered in 96-hour trajectories in each cluster. The West (W) includes tropical and warm polar maritime air masses formed over the Atlantic Ocean. The North (N) groups continental air masses originated over Europe, while there are polar maritime air masses generated over the Atlantic Ocean from high latitudes Northwest (NW). The Arctic air masses are characterized by cold air that originates from the polar regions near the Arctic Circle. They are characterized by extremely low temperatures and typically form during the winter months, as well as Mediterranean (Med) mixed warm continental air masses over the Mediterranean Sea and tropical continental air masses from Africa; and finally, South (S) includes continental and tropical maritime air masses arriving from the south. To determine the link of back-trajectories clusters with gross α and gross β peaks concentrations, the six activity ranges have been considered.

The back-trajectories analysis shows that the dominant air masses reaching the Granada atmosphere are those coming from the North (N), Northwest (NW), and West (W). Although these air masses are characterized by a high-frequency distribution, most of them were accompanied by lower values of both indexes (lower half Activity concentrations < 50P), because the maritime air masses are depleted in crustal radionuclides and moreover favour the wet scavenging of residual crustal component from far continental sources, thus decreasing the gross α and gross β activity concentrations (Russo and Borras, 2022). As the Activity increases (> 50P), the impact of the southern (S) and Mediterranean (Med) air masses is more evident. These air masses are the ones most contributing gross α and gross β emitters to Granada. Indeed, The Mediterranean cluster shows a high-frequency distribution at the shallowest altitude (750m); on the contrary, cluster (S) has a clear contribution from the highest altitude (3000 m).

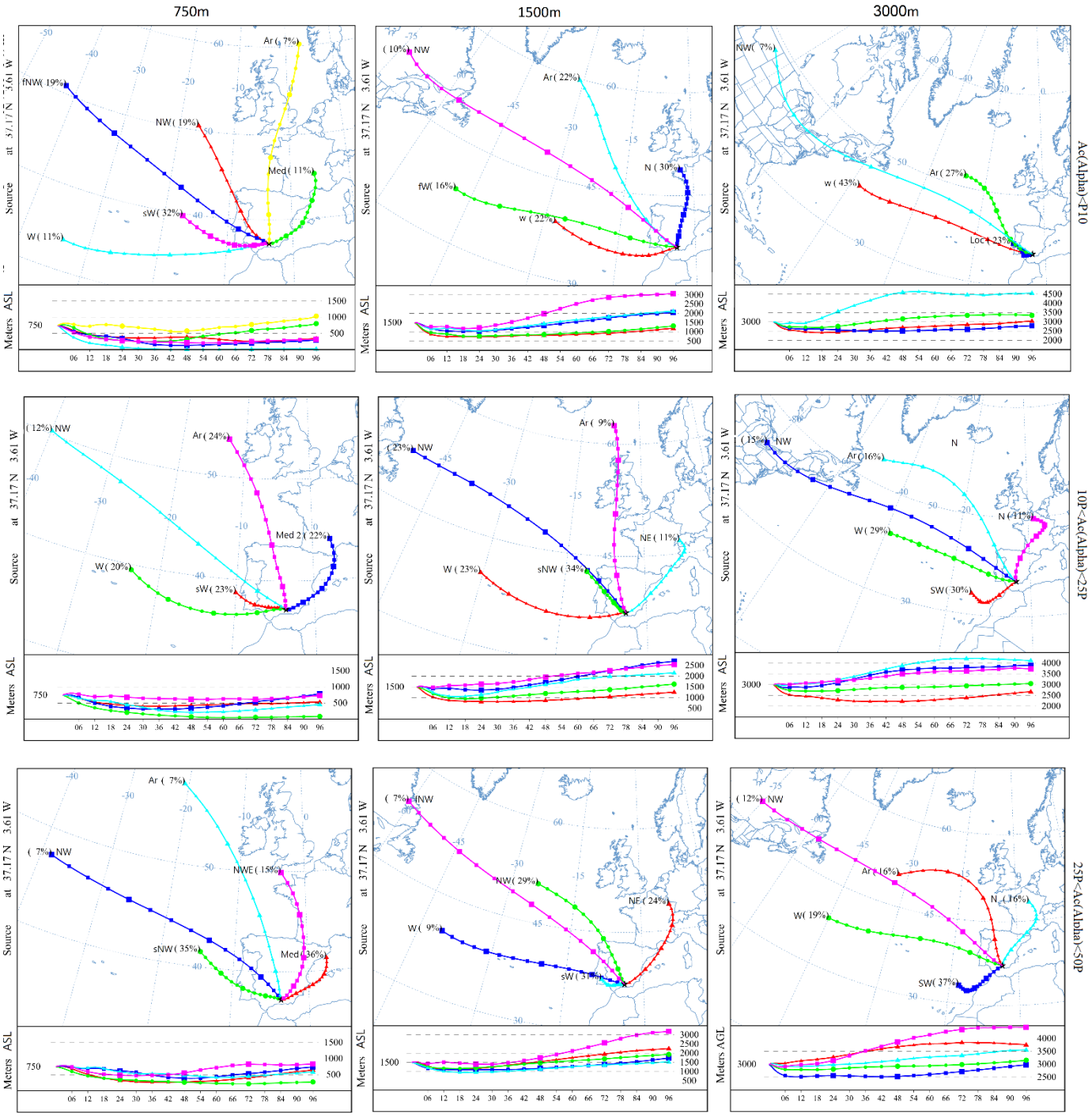

Figure 5: Back-trajectory analysis obtained at three altitudes over Granada: 750m, 1500m, and 3000m a.s.l for the six α activity ranges from 2006 to 2021.

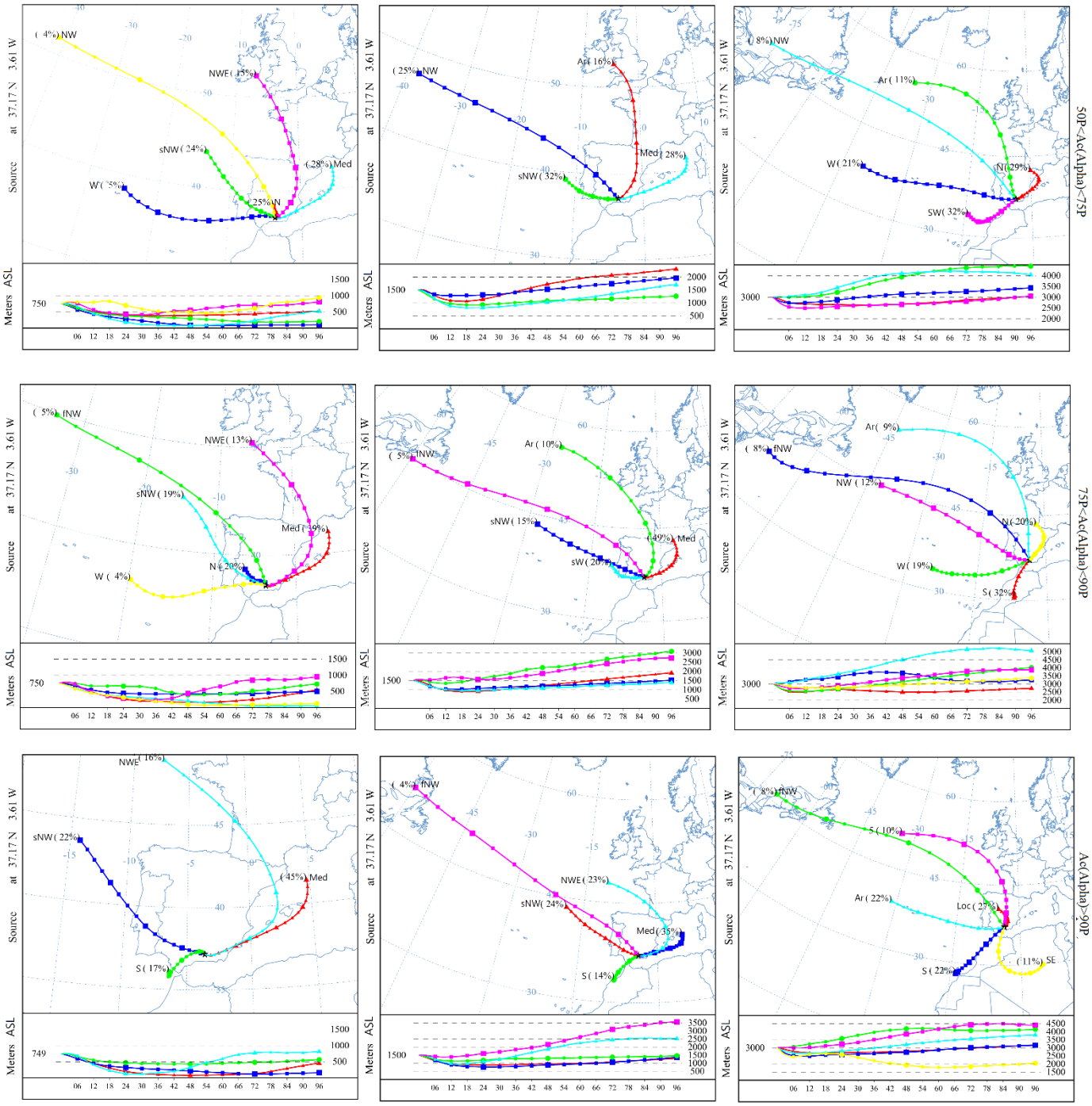

Figure 5: (continued)

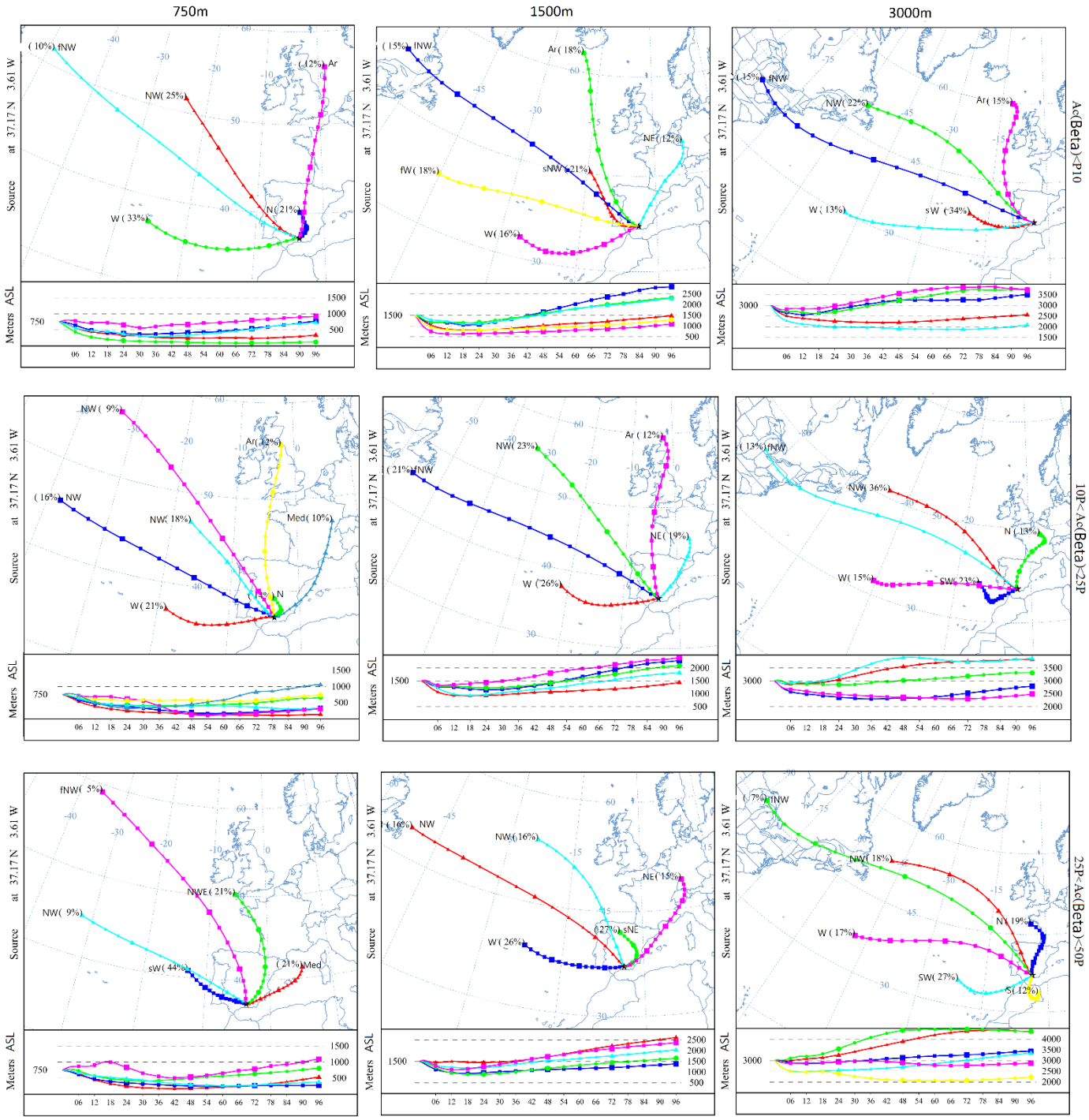

Figure 6: Back-trajectory analysis obtained at three altitudes over Granada: 750m, 1500m, and 3000m a.s.l for the six β activity ranges from 2006 to 2021.

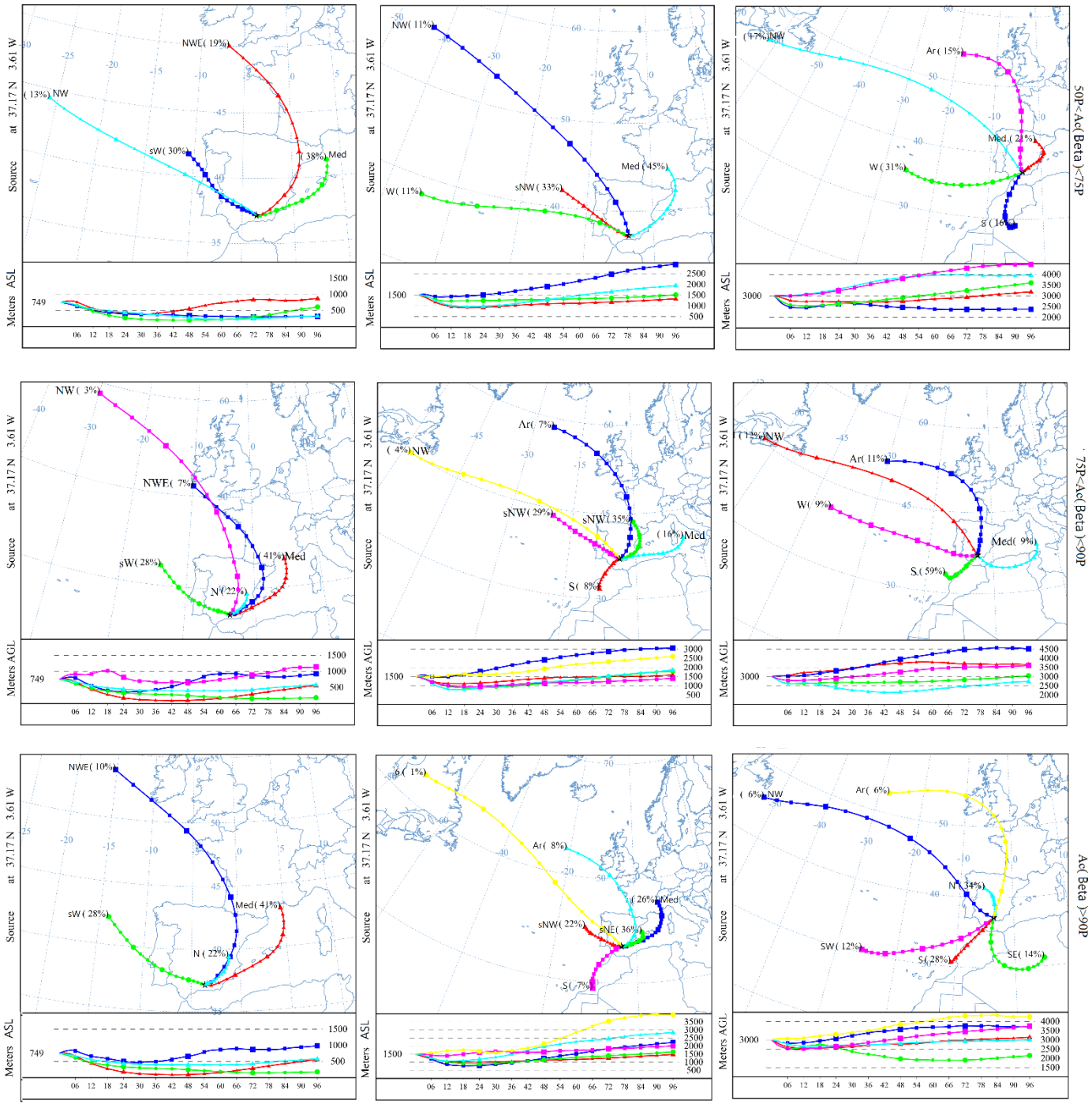

Figure 6: (continued)

It is essential to highlight that certain air masses originating from the north (N, NE) are linked to low gross α and gross β activity events, despite the fact that their paths pass over land before reaching Granada. This association can be attributed to the occurrence of significant wet scavenging along their trajectories, which results in aerosol depletion. This effect is illustrated in Figure 7, which reports the percentage of trajectories with relative humidity above 95% along their pathway together with the average humidity of the trajectories, for each activity range and each altitude. In this case, we have used only the last 48h of the back-trajectories before reaching the sampling site. This choice of 48h is based on the fact that wet deposition in proximity to the study site has more impact than further away. RH above 95% along the

trajectory has been used as a useful, rough, proxy of the wet scavenging effect at the height of the displacing air parcels, as they are close to water vapor saturation. In fact, we have manually analysed a large number of cases by using a more complete criteria: RH above 95% at points where the trajectory is well above the marine surface, and there is a reduction in specific humidity. With these criteria, ERA5 precipitation (at the ground level) shows rainfall below the air parcel location in most cases, and the corresponding activity concentrations were low. Rainfall (at the ground) is not an available parameter in the ERA-Interim database. We have found that precipitation not far from the study site (i.e., in northern Morocco, southwestern Iberian Peninsula, the northern slope of Sierra Nevada or directly over Granada) is associated with the lowest 10th percentile of activity concentrations and that precipitation at the northern slopes of the Cantabrian Mountain range and in the northern part of the Pyrenees where linked to the 10-25 and 25-50, percentile, respectively, for gross β activity concentrations. Rainfall was associated to the passage of cold fronts and to orographic precipitation. In Supplementary Material are included three examples.

Figure 7 shows that air masses corresponding to lower concentrations of gross α and gross β activity concentrations are extremely humid. As the concentration increases, the humidity decreases. The results presented in Figure 7 highlight the inverse relationship between gross α and gross β activity concentrations and humidity, indicating that the presence of humidity efficiently removes radioactive particles in the atmosphere, a factor very well known in the case of artificial radioactive fallout observed for weapon testing as well as for the reported accidents such as Chernobyl or naturally occurring radionuclides (Battiston et al., 1987; Tositti et al., 2020).

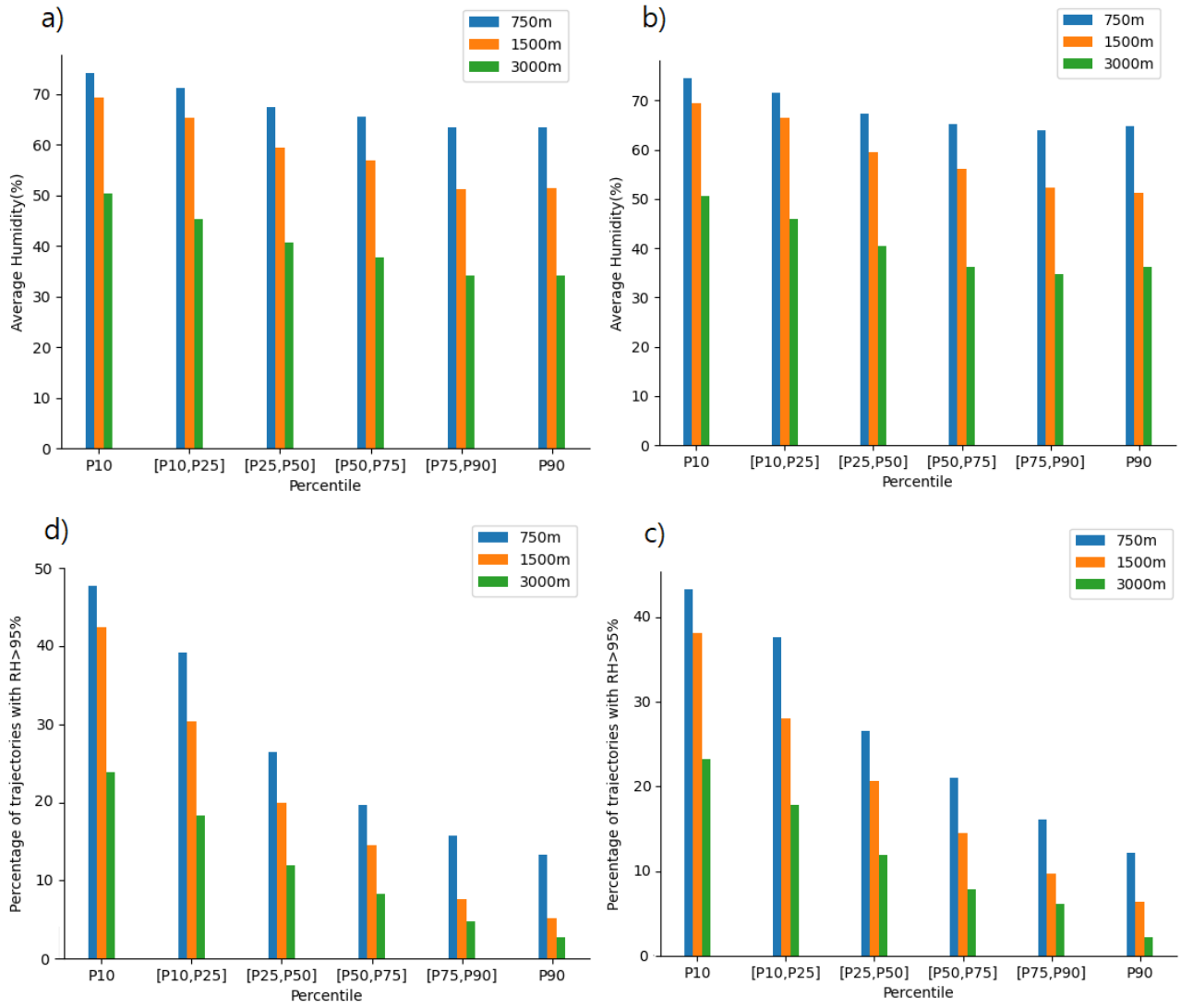

Figure 7: Average Humidity of the back-trajectories (a) for gross Alpha and (b) for gross Beta, Percentage of trajectories which have RH >95% (c) for gross Alpha and (d) for gross Beta, at three altitudes: 750m, 1500m, and 3000m a.s.l. and for six activity ranges from 2006 to 2021.

To identify the impact of each region on the measured concentrations, we have combined all clusters corresponding to each altitude and which have a similar origin. As gross α and gross β have a log normal and normal distribution, respectively, Spearman and Pearson correlations were applied respectively to assess the influence of the combined clusters. A positive correlation coefficient indicates that an increase in carrier aerosol concentration is related to the more frequent arrival of a particular air mass. On the other hand, a negative correlation value indicates a decrease in aerosol concentration with a higher arrival frequency of a type of air masses (Dueñas et al., 2011b).

The correlation coefficients between weekly activities of gross α and gross β activity concentrations and the combined clusters arriving at 750, 1500 and 3000 m have been calculated and reported in the table of correlations in the supplementary material. Only the highest values of correlation coefficients are

highlighted. The monthly trajectory density plots of the interesting clusters compared with the seasonality of gross α and gross β activities are presented in Figure 8.

According to table of correlations (supplementary material), there is a positive correlation between the activity concentrations of gross α and gross β activity concentrations and the air masses passing over the Mediterranean Sea at low altitude (Med 750m). The correlation coefficients for gross α and gross β are 0.3 and 0.52, respectively. The density plot of these air masses confirms this finding by showing similar variations in gross α and gross β concentrations with the density of the Mediterranean Sea (Figure 8). In months when the proportion of Med air masses is high, there is an increase in both gross α and gross β concentrations, and vice versa. As previously reported in clustering results, as the altitude increases, the influence of the Mediterranean cluster decrease, resulting in a decrease in correlation. Where, at 1500m, the correlation coefficients drop to 0.1 and 0.13 for gross α and gross β respectively. At high altitude (3000m), the significance of the Med cluster fades completely. However, there is a positive correlation observed with air masses originating from the south, specifically Northern Africa and the Sahara Desert, which are 0.29 and 0.43 for gross α and gross β, respectively. This cluster shows also a similar seasonality of gross α and gross β activity concentrations (Figure 8), which have a higher frequency in the summer months and a lower in the winter months. Furthermore, gross α and gross β exhibit a negative correlation with air masses from the Atlantic Ocean (NW, W), as well as with Arctic air masses originating from the polar regions. Unlike the Mediterranean and south air masses, these air masses are more frequent during winter months and less prevalent during summer months. This contrasting pattern persists across all altitudes. For the sake of brevity, the density plots for 750m are only presented to avoid repetition in Figure 8.

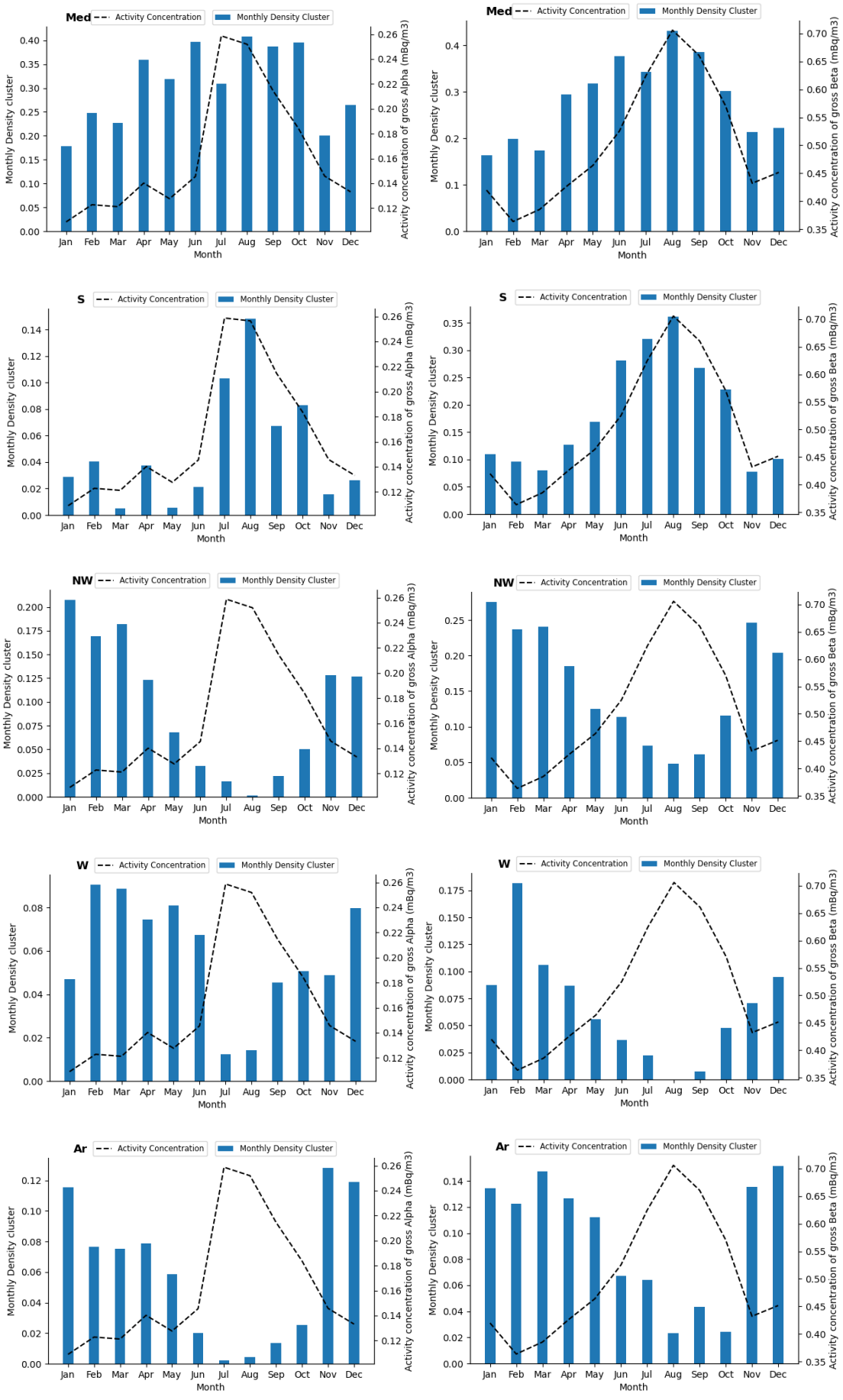

Figure 8: Monthly trajectory density plots showing the seasonal change of clusters compared with the identified seasonality of α and β activity.

The results obtained indicate a significant relationship between air masses, coming from the Mediterranean and the south (North Africa), and high concentrations of gross α and gross β activity. North Africa is characterized by wide arid regions in connection with a hot desert climate with minimal rainfall.
These dry environments, with low relative humidity (~10%) and high summer temperatures reaching 60°C, create favorable conditions for the re-suspension of substantial quantities of mineral dust. Consequently, intense surface heating during the day generates strong vertical thermal turbulence, extending up to altitudes of 4000 meters (Dubief, 1977). This turbulence is followed by periods of atmospheric stability induced by nocturnal thermal inversions. This scenario is a major source of crustal emissions (mineral dust), which are then transported over long distances. This makes the Sahara Desert the major source of mineral aerosols on the global scale (Gordo et al., 2015).
These conditions may explain the contribution of air masses from the south that reach high altitudes (3000 meters) and carry gross alpha-beta emitters (Tositti et al., 2014).

The influence of the Mediterranean Sea is noticeable. Although ^{222}Rn exhaled by the oceans contributes to only 2% of the atmospheric standing stock of ^{222}Rn, (Dueñas et al., 2004; Tositti et al., 2013, 2014) the Mediterranean sea is considered a reservoir of aged aerosols rich radionuclide as previously shown for ^{210}Pb by Brattich et al. (2016). It is also influenced by Saharan inputs, receiving substantial annual amounts of mineral particles. The average annual input of Saharan dust into the western Mediterranean has been estimated about 12.5 tons per square kilometer, with significant interannual variability. (Loÿe-Pilot et al. 1996). Therefore, Mediterranean and meridional air masses reaching Granada carry significant amounts of α and β radionuclides attached to mineral dust during the Saharan incursions.
Additionally, the air masses associated with higher concentrations of gross alpha beta radiation appear to be associated with Maroc addressing to local geological background in specific areas as reported in the next section.
The clustering analysis divides the trajectories into subgroups with well-distinct characteristics and origins, providing the identification of the clusters dominant in each week. In fact, the fast transient events happening within the duration of the sampling can affect the result of the trajectory analysis. However, in this work, this was counteracted by the large number of samples analyzed: indeed, here we utilized long-term measurements of gross α and gross β as a large database of more than 800 samples (weeks). The results indicate a clear difference between the cluster types contributing to high and low concentration.

3.4 Source Areas of gross α and gross β activities

To evaluate the accuracy of previous results, the WCWT model has been used. Figure 9 shows the distribution of WCWT values of gross α and gross β activities for each of the three studied altitudes. The colors present the weighted average concentration in a cell. According to the result displayed in Figure 9, at

the lowest altitude (750m), the highest WCWT values of gross α and gross β are mainly found in Northern Africa, southern France, as well as in the Mediterranean. On the other hand, the regions located in the Atlantic Ocean appear as poor sources of gross α and gross β emitters (low WCWT value). As the altitude increases, higher values of WCWT appear in the southern regions, while those of the Mediterranean coast are reduced. The same trends already emerged from the cluster analysis and Pearson/Spearman correlation. Moreover, the findings of the WCWT bring a new aspect by revealing that the southern France region can also have a significant contribution to gross alpha and beta activities. According to maps provided by the European Atlas of Natural Radiation, which has been developed and is being maintained by the Joint Research Centre (JRC) of the European Commission, this region is rich in uranium in the soil and has a high radon flux that can be transported by air masses arriving at Granada from this region.

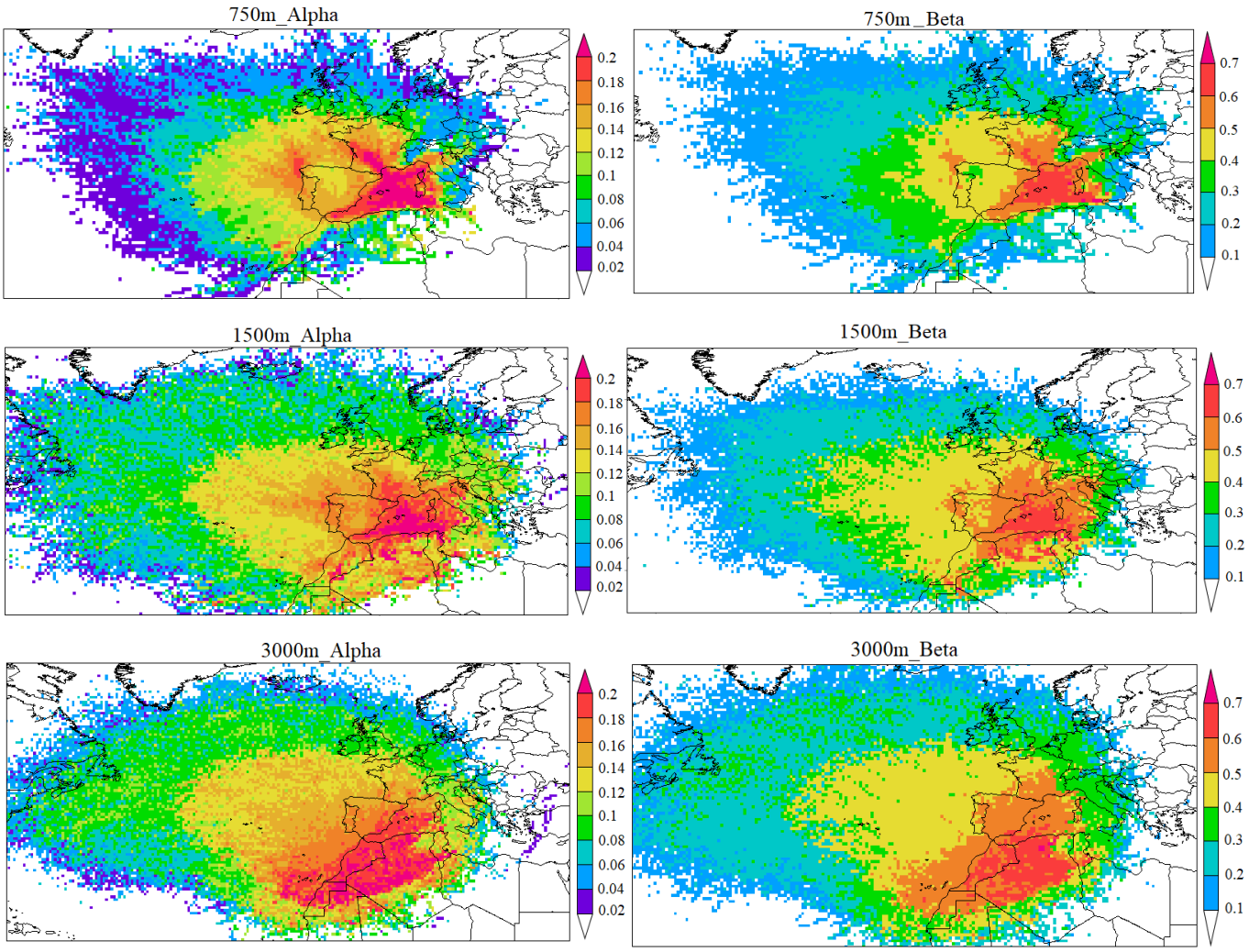

Figure 9: WCWT values of gross α (left column) and gross β (right column) indexes at 750, 1500 and 3000m (from top to bottom) during the study period.

4. Conclusion

The current research focuses on the influence of both local meteorological parameters and air masses (long-range transport) on atmospheric gross α and gross β activity concentrations, acquired weekly during an extended time interval of 16 years (2006-2021) at Granada, Spain.

After analyzing all results, the following conclusions can be drawn:

- Gross α and gross β activities concentration present cyclical variability that occurs each year, with the highest concentrations recorded in summer and the lowest values measured in winter.
- The use of decomposition time series has shown to be a powerful technique to determine which component was responsible for different patterns of gross α and gross β variability, considering their relation with atmospheric parameters. The results show that temperature (T) displayed a strong positive correlation with the seasonal component, while wind speed (WS) was strongly negatively correlated with the same component.
- The contradiction between the trend component of gross beta (which goes up) and that of gross alpha (which goes down) over the period of the study was unexpected and it will be analyzed in a future study where several sampling points with more impact parameters will be considered.
- The Continuous Wavelet Transform (CWT) analysis has been used to identify the periodicities expected from the trend component. The results indicated that the strong periodicities were smaller compared with the periodicities of the trend component.
- The analysis of back trajectories demonstrates the impact of long-range transport on radioactivity levels measured. The results obtained indicate a significant relationship between air masses coming from the Mediterranean and the south spatially North Africa, and high concentrations of gross α and gross β activity. Conversely, the low values of gross α and gross β are strongly associated to the air masses coming from northwest (Atlantic Ocean) and from polar regions (Arctic) which reduce the radioactivity measured in the atmosphere. Furthermore, the correlation between the combined clusters which have a similar origin and gross α and gross β activities, as well as the WCWT method confirmed that the ground level concentrations are influenced by the altitude of the air masses. In particular, the activity concentrations increase with the arrival of air masses from Mediterranean (low altitude, 750m) and from African (high altitude, 3000m) continent.
- The hourly or higher resolution data, such as spectral analysis of hourly wind speed or pressure observations, could provide more insights into the typical synoptic timescales at our study site. For this reason, will consider incorporating higher resolution data in future studies to better understand the influences of local and synoptic meteorology on our observations.

References

Bas, M.C., Ortiz, J., Ballesteros, L., Martorell, S., 2016. Analysis of the influence of solar activity and atmospheric factors on 7Be air concentration by seasonal-trend decomposition. Atmospheric Environment 145, 147-157. https://doi.org/10.1016/j.atmosenv.2016.09.027.

Battiston, G.A., Degetto, S., Gerbasi, R., Sbrignadello, G., Tositti, L., Croatto, U., 1987. The deposition of chernobyl fallout in North-east Italy. Inorganica Chimica Acta 140, 327-329. https://dx.doi.org/10.1016/S0020-1693(00)81115-9

Berriban, I., Azahra, M., Chham, E., Ferro-García, M.A., Milena-Pérez, A., Nouayti, A., Orza, J.A.G., Brattich, E., Tositti, L., Piñero-García, F., El Bardouni, T., Ziani, H., El Yaakoubi, H., El Barbari, M., 2022. PSCF and CWT methods as a tool to identify potential sources of 7Be and 210Pb aerosols in Granada, Spain. Journal of Environmental Radioactivity 251-252, 106977. https://doi.org/10.1016/j.jenvrad.2022.106977

Bossew, P., 2010. Radon: exploring the log-normal mystery. Journal of Environmental Radioactivity 101, 826-834. https://doi.org/10.1016/j.jenvrad.2010.05.005.

Brattich, E., Hernández-Ceballos, M.A., Orza, J.A.G., Bolívar, J.P., Tositti, L., 2016. The western Mediterranean basin as an aged aerosols reservoir. Insights from an old-fashioned but efficient radiotracer. Atmospheric Environment 141, 481-493. https://doi.org/10.1016/j.atmosenv.2016.07.022.

Brattich, E., Liu, H., Tositti, L., Considine, D.B., Crawford, J.H., 2017. Processes controlling the seasonal variations in 210Pb and 7Be at the Mt. Cimone WMO-GAW global station, Italy: a model analysis. Atmos. Chem. Phys. 17, 1061-1080. https://doi.org/10.5194/acp-17-1061-2017, 2017.

Brattich, E., Orza, J.A.G., Cristofanelli, P., Bonasoni, P., Marinoni, A., Tositti, L., 2020. Advection pathways at the Mt. Cimone WMO-GAW station: Seasonality, trends, and influence on atmospheric composition. Atmospheric Environment 234, 117513. https://doi.org/10.1016/j.atmosenv.2020.117513

Brattich, E., Liu, H., Zhang, B., Hernández-Ceballos, M.Á., Paatero, J., Sarvan, D., Djurdjevic, V., Tositti, L., Ajtić, J., 2021. Observation and modeling of high-7Be concentration events at the surface in northern Europe associated with the instability of the Arctic polar vortex in early 2003. Atmos. Chem. Phys. 21, 17927-17951. https://doi.org/10.5194/acp-21-17927-2021.

Cabello, M., Dueñas, C., Liger, E., Gordo, E., Cañete, S., 2018. Variables influencing the gross alpha and gross beta activities in airborne particulate samples in Málaga, Spain. Journal of radioanalytical and nuclear chemistry 315, 299-307. https://doi.org/10.1007/s10967-017-5674-3.

Chambers, S.D., Choi, T., Park, S.J., Williams, A.G., Hong, S.B., Tositti, L., Griffiths, A.D., Crawford, J., Pereira, E., 2017. Investigating Local and Remote Terrestrial Influence on Air Masses at Contrasting Antarctic Sites Using Radon-222 and Back Trajectories. Journal of Geophysical Research: Atmospheres 122, 13,525-513,544. https://doi.org/10.1002/2017JD026833.

Chambers, S.D., Preunkert, S., Weller, R., Hong, S.-B., Humphries, R.S., Tositti, L., Angot, H., Legrand, M., Williams, A.G., Griffiths, A.D., 2018. Characterizing atmospheric transport pathways to Antarctica

and the remote Southern Ocean using radon-222. Frontiers in Earth Science 6, 190. https://doi.org/10.3389/feart.2018.00190.

Chen, R., Peng, R. D., Meng, X., Zhou, Z., Chen, B., & Kan, H. 2013. Seasonal variation in the acute effect of particulate air pollution on mortality in the China Air Pollution and Health Effects Study (CAPES). Science of the total environment, 450, 259-265. https://doi.org/10.1016/j.scitotenv.2013.02.040

Cheng, I., Zhang, L., Blanchard, P., Dalziel, J., Tordon, R., 2013. Concentration-weighted trajectory approach to identifying potential sources of speciated atmospheric mercury at an urban coastal site in Nova Scotia, Canada. Atmos. Chem. Phys. 13, 6031-6048. https://doi.org/10.5194/acp-13-6031-2013.

Daubechies, I., 1990. The wavelet transform, time-frequency localization and signal analysis. IEEE transactions on information theory 36, 961-1005. 10.1109/18.57199.

Draxler, R., Stunder, B., Rolph, G., Taylor, A., 2009. HYSPLIT_4 User's Guide, via NOAA ARL website. NOAA Air Resources Laboratory, Silver Spring, MD, December 1997, revised January 2009.

Dueñas, C., Fernández, M.C., Carretero, J., Liger, E., Cañete, S., 2004. Long-term variation of the concentrations of long-lived Rn descendants and cosmogenic 7Be and determination of the MRT of aerosols. Atmospheric Environment 38, 1291-1301. https://doi.org/10.1016/S1352-2310(99)00172-7

Dueñas, C., Fernández, M.C., Gordo, E., Cañete, S., Pérez, M., 2011a. Gross alpha, gross beta activities and gamma emitting radionuclides composition of rainwater samples and deposition to ground. Atmospheric Environment 45, 1015-1024. https://doi.org/10.1016/j.atmosenv.2003.11.029

Dueñas, C., Fernández, M.C., Liger, E., Carretero, J., 1999. Gross alpha, gross beta activities and 7Be concentrations in surface air: analysis of their variations and prediction model. Atmospheric Environment 33, 3705-3715. https://doi.org/10.1016/j.atmosenv.2010.10.045

Dueñas, C., Orza, J.A.G., Cabello, M., Fernández, M.C., Cañete, S., Pérez, M., Gordo, E., 2011b. Air mass origin and its influence on radionuclide activities (7Be and 210Pb) in aerosol particles at a coastal site in the western Mediterranean. Atmospheric Research 101, 205-214. https://doi.org/10.1016/j.atmosres.2011.02.011

Fernández, A., Sainz, C., Celaya, S., Quindós, L., Rábago, D., Fuente, I., 2021. A New Methodology for Defining Radon Priority Areas in Spain, International Journal of Environmental Research and Public Health. https://doi.org/10.3390/ijerph18031352

García, Francisco Piñero, and M. Angeles Ferro García. 2014. Influence of Air Masses Origin on Radioactivity in Aerosols. 2nd Iberian Meeting on Aerosol Science and Technology: Proceedings Book RICTA, Universitat Rovira i Virgili Campus Catalunya, Spain, pp. 73-77.

García-Talavera, M., Quintana, B., García-Díez, E., Fernández, F., 2001. Studies on radioactivity in aerosols as a function of meteorological variables in Salamanca (Spain). Atmospheric Environment 35, 221-229. https://doi.org/10.1016/S1352-2310(00)00234-X

García-Talavera, S., Acevedo, F., 2019. CSN Technical Reports Collection 51.2019. INT-04.41 Cartography of Radon Potential in Spain. Nuclear Safety Council (CSN).

Gordo, E., Liger, E., Dueñas, C., Fernández, M.C., Cañete, S., Pérez, M., 2015. Study of 7Be and 210Pb as radiotracers of African intrusions in Malaga (Spain). Journal of Environmental Radioactivity 148, 141-153. https://doi.org/10.1016/j.jenvrad.2015.06.028

Guerrero-Rascado, J.L., Olmo, F., Avilés-Rodríguez, I., Navas-Guzmán, F., Pérez-Ramírez, D., Lyamani, H., Alados Arboledas, L., 2009. Extreme Saharan dust event over the southern Iberian Peninsula in

september 2007: active and passive remote sensing from surface and satellite. Atmospheric Chemistry and Physics 9, 8453-8469. https://doi.org/10.5194/acp-9-8453-2009

Hernández-Ceballos, M.A., Brattich, E., Ajtić, J., 2022. Airflow and teleconnection patterns driving the spatial and temporal variability of high 7Be air concentrations in Europe. Chemosphere 303, 135194. https://doi.org/10.1016/j.chemosphere.2022.135194

Hernández, F., Hernández-Armas, J., Catalán, A., Fernández-Aldecoa, J.C., Karlsson, L., 2005. Gross alpha, gross beta activities and gamma emitting radionuclides composition of airborne particulate samples in an oceanic island. Atmospheric Environment 39, 4057-4066. https://doi.org/10.1016/j.atmosenv.2005.03.035

Hirose, K., 2012. Uranium, thorium and anthropogenic radionuclides as atmospheric tracers. Handbook of Environmental Isotope Geochemistry: Vol I, 591-611.

Keim, B.D., Muller, R.A., Stone, G.W., 2004. Spatial and temporal variability of coastal storms in the North Atlantic Basin. Marine Geology 210, 7-15. https://doi.org/10.1016/j.margeo.2003.12.006

Lee, H.N., Tositti, L., Zheng, X., Bonasoni, P., 2007. Analyses and comparisons of variations of 7Be, 210Pb, and 7Be/210Pb with ozone observations at two Global Atmosphere Watch stations from high mountains. Journal of Geophysical Research: Atmospheres 112. https://doi.org/10.1029/2006JD007421

Loÿe-Pilot, M., Martin, J., 1996. Saharan dust input to the western Mediterranean: an eleven years record in Corsica. The impact of desert dust across the Mediterranean, 191-199.

Morozzi, P., Ballarin, B., Arcozzi, S., Brattich, E., Lucarelli, F., Nava, S., Gómez-Cascales, P.J., Orza, J.A.G., Tositti, L., 2021. Ultraviolet–Visible Diffuse Reflectance Spectroscopy (UV–Vis DRS), a rapid and non-destructive analytical tool for the identification of Saharan dust events in particulate matter filters. Atmospheric Environment 252, 118297. https://doi.org/10.1016/j.atmosenv.2021.118297

Okkaoğlu, Y., Akdi, Y., & Ünlü, K. D. 2020. Daily PM10, periodicity and harmonic regression model: The case of London. Atmospheric Environment, 238, 117755. https://doi.org/10.1016/j.atmosenv.2020.117755

Papastefanou, C., 2008. Chapter 2 Radioactive aerosols, in: Papastefanou, C. (Ed.), Radioactivity in the Environment. Elsevier, pp. 11-58. https://doi.org/10.1016/S1569-4860(07)12002-7

Piñero-García, F., Ferro-García, M.Á., 2014. Influence of Air Masses Origin on Radioactivity in Aerosols, 2nd Iberian Meeting on Aerosol Science and Technology. Publicacions Universitat Rovira I Virgili, p. 73. https://doi.org/10.1016/j.jenvrad.2015.05.029

Piñero-García, F., Ferro-García, M.A., Chham, E., Cobos-Díaz, M., González-Rodelas, P., 2015. A cluster analysis of back trajectories to study the behaviour of radioactive aerosols in the south-east of Spain. Journal of Environmental Radioactivity 147, 142-152. https://doi.org/10.1016/j.jenvrad.2015.05.029

Reiter, R., Munzert, K., 1982. Results of synchronous and unbroken measurements of natural atmospheric radioactivity from 1964 1979 at three stations (0.7 3.0 km asl) and review of the initial studies from 1956 on. Archives for Meteorology Geophysics and Bioclimatology Series B Theoretical and Applied Climatology 31, 39-64. 10.1007/BF02311341

Russo, A., Borras, A., 2022. Comparison of dimension reduction techniques applied to the analysis of airborne radionuclide activity concentration. Journal of Environmental Radioactivity 244-245, 106813. https://doi.org/10.1016/j.jenvrad.2022.106813

Sáez-Muñoz, M., Bas, M.d.C., Ortiz, J., Martorell, S., 2018. Analysis of the evolution of gross alpha and gross beta activities in airborne samples in Valencia (Spain). Journal of Environmental Radioactivity 183, 94-101. https://doi.org/10.1016/j.jenvrad.2017.12.019

Scott, M., Chandler, R., 2011. Statistical methods for trend detection and analysis in the environmental sciences. John Wiley & Sons.

Sykora, I., Froehlich, K., 2009. Chapter 3 Radionuclides as Tracers of Atmospheric Processes, in: Froehlich, K. (Ed.), Radioactivity in the Environment. Elsevier, pp. 51-88. https://doi.org/10.1016/S1569-4860(09)01603-9

Terray, L., D'Amico, D., Masson, O., Sabroux, J.-C., 2020. What can gross alpha/beta activities tell about 210Po and 210Pb in the atmosphere? Journal of Environmental Radioactivity 225, 106437. https://doi.org/10.1016/j.jenvrad.2020.106437

Titos, G., Lyamani, H., Cazorla, A., Sorribas, M., Foyo-Moreno, I., Wiedensohler, A., Alados-Arboledas, L., 2014. Study of the relative humidity dependence of aerosol light-scattering in southern Spain. Tellus B: Chemical and Physical Meteorology 66, 24536. https://doi.org/10.3402/tellusb.v66.24536

Tositti, L., Brattich, E., Cinelli, G., Baldacci, D., 2014. 12 years of 7Be and 210Pb in Mt. Cimone, and their correlation with meteorological parameters. Atmospheric Environment 87, 108-122. https://doi.org/10.1016/j.atmosenv.2012.10.051

Tositti, L., Moroni, B., Dinelli, E., Morozzi, P., Brattich, E., Sebastiani, B., Petroselli, C., Crocchianti, S., Selvaggi, R., Enzo, G., Cappelletti, D., 2020. Deposition processes over complex topographies: Experimental data meets atmospheric modeling. Science of The Total Environment 744, 140974. https://doi.org/10.1016/j.atmosenv.2014.01.014

Tositti, L., Riccio, A., Sandrini, S., Brattich, E., Baldacci, D., Parmeggiani, S., Cristofanelli, P., Bonasoni, P., 2013. Short-term climatology of PM10 at a high altitude background station in southern Europe. Atmospheric Environment 65, 142-152. https://doi.org/10.1016/j.scitotenv.2020.140974

Turekian, K.K., Graustein, W.C., 2003. 4.10 - Natural Radionuclides in the Atmosphere, in: Holland, H.D., Turekian, K.K. (Eds.), Treatise on Geochemistry. Pergamon, Oxford, pp. 261-279. 10.1016/B0-08-043751-6/04042-1

Vargas, A., Arnold, D., Adame, J.A., Grossi, C., Hernández-Ceballos, M.A., Bolivar, J.P., 2015. Analysis of the vertical radon structure at the Spanish "El Arenosillo" tower station. Journal of Environmental Radioactivity 139, 1-17. https://doi.org/10.1016/j.jenvrad.2014.09.018

WHO, 2009. WHO handbook on indoor radon: a public health perspective. World Health Organization.

Wu, X., He, S., Guo, J., & Sun, W. 2021. A multi-scale periodic study of PM2. 5 concentration in the Yangtze River Delta of China based on Empirical Mode Decomposition-Wavelet. Analysis Cleaner Production, 281, 124853. https://doi.org/10.1016/j.jclepro.2020.124853

885